Hemodynamic cerebral correlates of sleep spindles during human non-rapid eye movement sleep

M. Schabus[†‡§], T. T. Dang-Vu[†¶], G. Albouy[†], E. Balteau[†], M. Boly[†¶], J. Carrier[‖], A. Darsaud[†], C. Degueldre[†], M. Desseilles[†,††], S. Gais[†], C. Phillips[†], G. Rauchs[†], C. Schnakers[†], V. Sterpenich[†], G. Vandewalle[†], A. Luxen[†], and P. Maquet[†§¶]

[†]Cyclotron Research Centre, University of Liège, B-4000 Liège, Belgium; [††]Departments of Psychiatry and [¶]Neurology, Centre Hospitalier Universitaire de Liège, B-4000 Liège, Belgium; [‡]Department of Psychology, University of Salzburg, A-5020 Salzburg, Austria; and [‖]Department of Psychology, University of Montréal, Montréal, QC, Canada H3C 3J7

Edited by Marcus E. Raichle, Washington University School of Medicine, St. Louis, MO, and approved June 26, 2007 (received for review April 3, 2007)

In humans, some evidence suggests that there are two different types of spindles during sleep, which differ by their scalp topography and possibly some aspects of their regulation. To test for the existence of two different spindle types, we characterized the activity associated with slow (11–13 Hz) and fast (13–15 Hz) spindles, identified as discrete events during non-rapid eye movement sleep, in non-sleep-deprived human volunteers, using simultaneous electroencephalography and functional MRI. An activation pattern common to both spindle types involved the thalami, paralimbic areas (anterior cingulate and insular cortices), and superior temporal gyri. No thalamic difference was detected in the direct comparison between slow and fast spindles although some thalamic areas were preferentially activated in relation to either spindle type. Beyond the common activation pattern, the increases in cortical activity differed significantly between the two spindle types. Slow spindles were associated with increased activity in the superior frontal gyrus. In contrast, fast spindles recruited a set of cortical regions involved in sensorimotor processing, as well as the mesial frontal cortex and hippocampus. The recruitment of partially segregated cortical networks for slow and fast spindles further supports the existence of two spindle types during human non-rapid eye movement sleep, with potentially different functional significance.

electroencephalography (EEG)/functional MRI (fMRI) | light sleep | neuroimaging | sleep physiology

Human sleep is associated with a profound modification of consciousness and the emergence of distinct sleep oscillations. In the early stages of non-rapid eye movement (NREM) sleep, electroencephalographic recordings show characteristic spindle oscillations. In humans, spindles consist of waxing-and-waning 11- to 15-Hz oscillations, lasting 0.5–3 sec. At the cellular level, spindles are associated with substantial neuronal activity. Spindles arise from cyclic inhibition of thalamo-cortical (TC) neurons by reticular thalamic neurons. Postinihibitory rebound spike bursts in TC cells entrain cortical populations in spindle oscillations (1). These neuronal mechanisms, which involve large TC populations, are thought to shape the processing of information during light NREM sleep and participate in the alteration of consciousness that characterizes this stage of sleep.

Little is known on the cerebral correlates of human spindles. Early positron emission tomography studies reported a negative relationship between thalamic cerebral blood flow and the power spectrum in the spindle frequency band (2). However, the low temporal resolution of positron emission tomography did not allow for a fine-grained characterization of the cerebral correlates of human spindles. In addition, two kinds of spindles are described in humans. Slow spindles (<13 Hz) predominate over frontal, whereas fast spindles (>13 Hz) prevail over centro-parietal areas. The difference in spindle scalp topography is also reflected by profound functional differences. These two spindling activities differ by their circadian and homeostatic regulations, pharmacological reactivity, development in infancy, evolution during aging, modulation during menstrual cycle and pregnancy (3), and, intriguingly, by their association with general cognitive capabilities (4). Source reconstruction of scalp EEG recordings identified two sources, one for slow spindles in a mesial frontal region and another for fast spindles in the precuneus (5). Despite these functional differences, it is still debated whether slow and fast spindles reflect the activity of different neural networks or the differential modulation of a single generator (for review, see ref. 3).

In this article, we first aimed at characterizing the cerebral correlates of the neural activity associated with spindles, in a group of normal, young, and non-sleep-deprived volunteers, using simultaneous electroencephalography (EEG)/functional MRI (fMRI) acquisitions. EEG recordings allowed us to precisely identify the onsets of slow and fast spindles which were subsequently used in the fMRI analysis as in a classical event-related design. Second, we tested the hypothesis that in humans, there are two distinct spindle types by estimating the differences between the regional brain activity associated with slow and fast spindles.

Results

Of 25 subjects, 14 participants maintained stable S2 and S3 sleep periods (Fig. 1*a* for a representative EEG recording). In these subjects, the series of consecutive fMRI volumes corresponding to steady stage 2 or stage 3 NREM sleep were selected from the complete fMRI time series. They constituted a "session" and were considered for further analysis. One to six sessions [mean (SE): 3.5 (0.5)] were selected per subject [duration range: 137.8–2,164.8 sec, mean (SE): 622.9 sec (63.4)].

Based on previous data-driven analysis of human sleep data, it appears that the frequency that best separates slow from fast spindles is ≈13 Hz (5, 6). Consequently, slow and fast sleep spindles were identified on band pass-filtered data between 11–13 Hz and 13–15 Hz respectively, using an automatic detection algorithm inspired from Mölle *et al.* (7). The mean (SE) number of detected slow and fast sleep spindles per subject was 74.6 (10.6) and 95.3 (14.6), respectively. On average, 21.3 (2.14) slow and 27.2 (2.74) fast spindles were identified per session. As expected, the power in slow and fast sigma bands predominated respectively over frontal and centro-parietal scalp areas (Fig. 1*b*). Additionally, averaging 0.5–4

Author contributions: M.S., T.T.D.-V., and P.M. designed research; M.S., T.T.D.-V., G.A., M.B., J.C., A.D., M.D., S.G., G.R., C.S., V.S., G.V., and P.M. performed research; E.B., C.D., C.P., A.L., and P.M. contributed new reagents/analytic tools; M.S. and T.T.D.-V. analyzed data; and M.S. and P.M. wrote the paper.

The authors declare no conflict of interest.

This article is a PNAS Direct Submission.

Abbreviations: EEG, electroencephalography; fMRI, functional MRI; NREM, non-rapid eye movement; SMA, supplementary motor area; TC, thalamo-cortical.

[§]To whom correspondence may be addressed at: Cyclotron Research Centre, University of Liège, Belgium. E-mail: manuel.schabus@sbg.ac.at or pmaquet@ulg.ac.be.

This article contains supporting information online at www.pnas.org/cgi/content/full/0703084104/DC1.

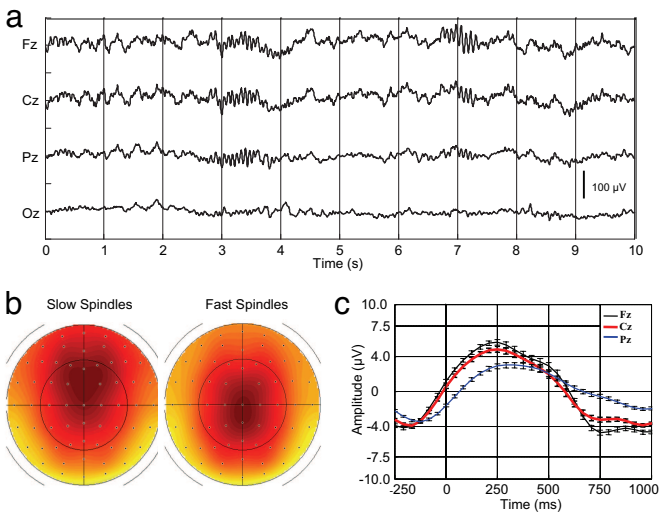

Fig. 1. EEG characterization of sleep spindles. (*a*) Example of a typical EEG recording (stage 2 sleep; 0.1 to 70 Hz) after scanner and pulse artifact correction, depicting a fast posterior (Pz, left side) and a slow anterior (Fz, right side) spindle. (*b*) EEG scalp topography of the average spindle band power between 11–13 (left) and 13–15 Hz (right). For display the average normalized spindle power of all slow and fast sleep spindles (detected on Cz) was computed at each channel and between 11–13 and 13–15 Hz, respectively. Slow sigma power predominates over frontal central regions whereas fast sigma power is mainly expressed over centro-parietal areas. Nose is upwards, right is rightwards. (*c*) Spindle-triggered average revealing the underlying slow oscillation. EEG data (0.5–4 Hz) were averaged with respect to the onset of all sleep spindles. Spindles start (t = 0) on the depolarizing phase of the oscillation, which on average are of much smaller amplitude than the classical full blown slow waves of deep slow-wave sleep. The classical phase lag from frontal (Fz, black) to central (Cz, red) and parietal (Pz, blue) areas and the maximal slow wave amplitude at the frontal recording site are also depicted.

Hz filtered EEG recordings with respect to spindle onsets confirmed that spindles occurred on the depolarizing phase of the slow oscillation (7) (Fig. 1*c*).

We first identified the brain areas responding to both slow and fast spindles (conjunction analysis: Fig. 2 and Table 1, center columns). Significant positive responses were identified in the left and right thalamus in their lateral and posterior aspects. At the cortical level, significant increases in activity were detected in paralimbic areas: the anterior cingulate cortex and the left insula. In the neocortex, significant responses common to all spindles were identified bilaterally in the superior temporal gyrus, in the vicinity of auditory cortices.

Beyond these common activations, brain activity associated with slow and fast spindles did not overlap completely [main effect of each spindle type: Fig. 2 and Table 1, left and right columns; additional results in supporting information (SI) Tables 3 and 4]. The distribution of brain activity during slow spindles resembled the common activity pattern, with significant responses identified in the thalami, anterior cingulate, insular, and auditory cortices. There were two noticeable differences with the common activity pattern. First, at the thalamic level, the activity associated with slow spindles involved the largest part of thalami although it spared their anterior portion. Moreover, additional subcortical responses associated with slow spindles were observed in the floor of the third ventricle (basal forebrain/hypothalamus), the midbrain tegmentum, and cerebellar vermis. Second, at the cortical level, in addition to the common activity pattern, a single area showed a significant activity associated with slow spindles, in the right superior frontal gyrus.

In contrast to slow spindles, the activity related to fast spindles appeared limited at the thalamic level but more extended at the cortical level, relative to the common activity pattern. At the cortical level, in addition to the common activity pattern, significant activity related to fast spindles was detected not only in orbitofrontal and middle frontal areas, but interestingly also in the precentral and postcentral gyri, supplementary motor area (SMA), and in mid-cingulate cortex ventral to the cingulate motor zones (Fig. 2 and Table 1, right columns).

Finally, we directly compared the activities related to slow and fast sleep spindles. This differential effect conveys important information that does not necessarily appear in the simple main effects reported above. Importantly, we detected no significant difference in the thalamus (even at a lenient statistical threshold, $P < 0.01$ uncorrected). In contrast, at the cortical level, significant differential responses to fast (as compared with slow) spindles were mainly located in regions reported above as active during fast spindles, with significant responses identified in the orbital and middle frontal, precentral and postcentral, and insular cortices (Table 2; additional results in SI Table 5). Interestingly, larger activity for fast spindles was also observed within the mesial prefrontal cortex and hippocampus (Fig. 3).

The only region showing larger activity during slow than fast spindles was identified in the superior frontal gyrus. In line with the notion that slow spindles are usually more anteriorly located was the observation that thalamic peak voxels for slow spindles were primarily located in areas compatible with the mediodorsal nucleus (8), which has highest probability of connection with the prefrontal cortex (9). Furthermore, peak voxels for fast spindles were compatible with the ventral posterior lateral and pulvinar nuclei (8) having a substantial probability of connection (9) to primary sensorimotor, premotor and posterior parietal cortices (cf. SI Table 6). Consistent with these anatomical data, there was a significant linear relationship between the activity recorded in peak thalamic voxels [8 −16 4] for slow spindles and superior frontal gyrus (38 58 20, $Z = 3.38$, $P_{SVC} < 0.05$) as well as between the activity recorded in peak thalamic voxels for fast spindles [16 −22 6] and cingulate motor zones (6 −38 22, $Z = 4.29$; −2 −26 28, $Z = 3.94$, $P_{SVC} < 0.01$) and SMA (2 −8 66, $Z = 4.42$, $P_{SVC} < 0.01$).

Discussion

The cerebral correlates of slow and fast spindles, taken as discrete and identifiable neural events, were characterized by using EEG/fMRI in non-sleep-deprived normal human volunteers during the first part of the night. The main findings can be summarized in three points. First, an activation pattern common to both spindle types was identified, which involved both thalami, the anterior cingulate cortex, the left anterior insula, and, bilaterally, the superior temporal gyrus. Second, significant differences in cortical activations were observed between slow and fast spindles. The activity associated with slow spindles largely corresponded to the common activation pattern, with the additional recruitment of the right superior frontal gyrus. On the contrary, fast spindles were associated with a number of significant activations beyond the common pattern in the SMA, sensori-motor, and mid-cingulate cortex. Fast spindles elicited significantly larger responses than slow spindles in the left hippocampus the orbito and mesial prefrontal cortex, sensori-motor cortex, and anterior insula. Third, no significant difference in thalamic activation was detected when slow and fast spindles were directly compared with each other. Slow spindles were associated with a significant activation in the bulk of both thalami, with the exception of their anterior portion. Fast spindles were associated with a thalamic activation of smaller extent, although at lower statistical threshold, they also recruited a large part of both thalami.

Common Activation Pattern. As expected, significant responses were identified in the left and right thalami in keeping with the increase in firing during spindles reported at the cellular level (1). At the cortical level, significant increases in activity were detected in paralimbic areas: the left insula and the anterior cingulate cortex.

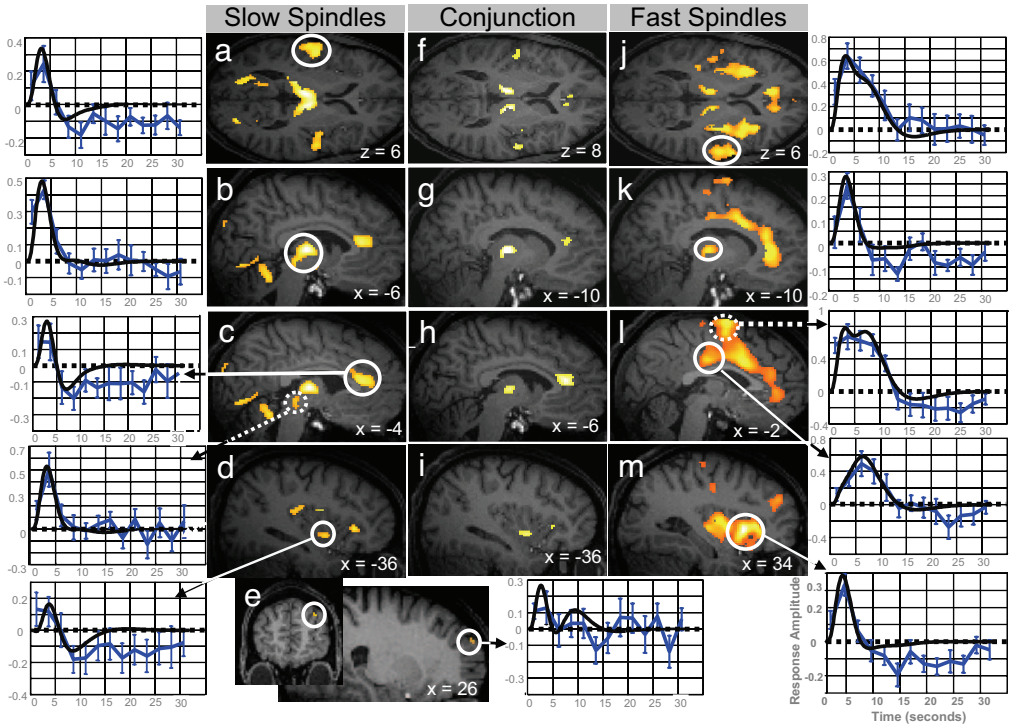

Fig. 2. Main effects of slow and fast sleep spindles. (*a–e Left*) fMRI responses to slow spindles displayed over an individual structural image normalized to the Montreal Neurological Institute space ($P_{uncorrected} < 0.001$). The leftmost panels show peristimulus time histograms (PSTHs) depicting the responses in auditory cortices (circled) (*a*), thalamus (b), anterior cingulate (circled) and midbrain tegmentum (dotted) (*c*), anterior insula (*d*), and superior frontal gyrus (e). The PSTH (solid blue line; blue error bars reflect the SEM) depicts the mean response across spindles of the corresponding voxel, irrespective of contrast based on a finite impulse response refit. The fitted response is drawn in black. (*f–i Center*) Conjunction analysis of slow and fast sleep spindles. (*j–m Right*) fMRI responses to fast spindles ($P_{uncorrected} < 0.001$). The rightmost panels show PSTHs depicting the response in superior temporal gyri (*j*), thalami (*k*), mid cingulate cortex (circled) and SMA (dotted) (*l*), and anterior insula (*m*).

The latter result contrasts with the assumption that spindles are absent in the cingulate cortex (ref 1, page 284). This notion was based on the observation that in cats, anterior thalamic nuclei, which project to cingulate cortex, do not receive inputs from the reticular nucleus (10) and do not show any spindling activity (11). In contrast, anterior cingulate and insular cortices seem deeply involved in human NREM sleep rhythms: Not only are they systematically active during both types of spindles (Fig. 2), but their activity is known to change significantly during deep NREM sleep (12, 13). During spindles, the anterior cingulate cortex might be driven by medio-dorsal (14) or intralaminar thalamic inputs. In the neocortex, significant responses common to all spindles were only identified in bilateral superior temporal gyri, in a location corresponding to auditory cortices. One might be tempted to attribute this activation to processing of scanner noise. This assumption would suggest that transmission of auditory inputs during sleep is modulated by spindles. Auditory information has been shown to be processed up to the cortical level during NREM sleep (15). However, changes in responses evoked by sounds presented during spindles, relative to outside spindles, suggest that spindles inhibit information processing and protect the sleeper from intrusive external stimuli (16). These results are consistent with the view, originating from animal experiments, that the brain is disconnected from the external world during NREM sleep because of synaptic inhibition in the thalamus (1). Future research should aim at further characterizing the cerebral correlates of sound processing during spindles.

Difference in Cortical Activity Associated with Slow and Fast Spindles. The cortical activity associated with slow spindles was essentially limited to the common activation pattern. However, an additional activity was identified in the superior frontal gyrus. As slow spindles are readily recorded from all prefrontal cortices in humans by electro-corticography (17), we expected a larger recruitment of frontal cortices in relation to slow spindles. However, in scalp EEG recordings, spindles show variable topographical dynamics over frontal regions (18), suggesting that any given prefrontal region does not systemically respond to each slow spindle, thereby reducing the probability of detection in our analysis.

Consistent responses to fast spindles were detected in a number of brain areas, on top of the common activation pattern. Several of these areas clustered around sensorimotor regions: sensori-motor cortices, SMAs, and mid-cingulate cortex. These findings are consistent with scalp EEG data suggesting that fast spindles are topographically and dynamically limited to central and parietal scalp areas (5, 18). Interestingly, these sensorimotor areas are also prone to oscillate in the 8–20 Hz range during wakefulness (19, 20). The sensorimotor (μ) rhythm is known as a conspicuous spontaneous rhythm of relaxed wakefulness, involving the sensorimotor and premotor cortices (19, 21). Although they differ in several respects (1), spindles and μ rhythm seem functionally related. Indeed, in cats, facilitation of sensorimotor rhythm through conditioning during wakefulness increases spindles and decreases motor output during subsequent sleep (22). Fast spindles might thus emerge from the interaction between the oscillatory properties of these sensorimotor TC loops and the oscillatory context of NREM sleep, characterized for instance by a slow rhythm (<1 Hz) which organizes the recurrence of spindles (7, 23).

The differential contrast between the two spindle types also revealed a larger recruitment of mesial-prefrontal and hippocampal areas during fast, relative to slow, spindles. This result might appear surprising as the hippocampus is not detected in the simple main effect of fast spindles. However, it is explained by the opposite time courses of hippocampal responses during slow and fast spindles (cf.

Table 1. Brain areas showing significant spindle-related increase in activity

Region	Slow spindles					Conjunction					Fast spindles				
	x	*y*	*z*	*Z* score	P_{SVC}	*x*	*y*	*z*	*Z* score	P_{SVC}	*x*	*y*	*z*	*Z* score	P_{SVC}
Midbrain tegmentum (13)	4	−28	−6	3.63	0.020										
Cerebellum (13)	−4	−54	−20	3.62	0.021										
	8	−60	−14	3.87	0.009										
Thalamus (13)	−4	−16	8	4.69	<0.001	−10	−18	6	4.06	0.005	12	−16	8	3.94	0.007
	8	−16	8	4.69	<0.001	12	−16	8	3.94	0.007	−10	−18	6	4.06	0.005
Basal forebrain/hypothalamus	−8	−2	−8	3.54	0.027										
(12, 13)	8	0	−6	3.57	0.024										
Orbito-frontal cortex (33)											28	24	−18	4.39	0.001
Superior Frontal Gyrus (30)	26	60	32	3.36	0.046										
Middle frontal gyrus (13, 34)											−38	42	22	3.87	0.009
											30	42	28	3.36	0.047
Supplementary motor area (33)											−2	0	62	4.07	0.004
Precentral gyrus (33)											−42	−6	36	3.34	0.048
Postcentral gyrus (33)											−54	−8	40	3.52	0.028
Anterior cingulate cortex	−6	34	14	4.14	0.004	−6	36	16	4.00	0.006	−4	14	32	4.76	<0.001
(12, 13)	6	38	12	3.72	0.015	8	38	12	3.70	0.016	−8	40	6	4.24	0.002
	−2	26	24	3.40	0.041										
Mid-cingulate cortex (33)											0	−22	32	3.73	0.015
											8	−36	26	3.4	0.041
Anterior insula (13)	−36	0	−6	3.52	0.029	−36	0	−6	3.52	0.029	−34	14	2	4.45	0.001
											34	14	−2	5.32	<0.001
Posterior insula (13)	−40	−24	22	3.67	0.018						−36	−28	4	3.77	0.013
											34	−18	0	4.14	0.004
Superior temporal gyrus (33)	−56	−6	6	4.01	0.006	−62	0	2	3.39	0.049	−46	−14	6	3.45	0.035
	54	−8	4	3.67	0.018	56	−10	6	3.51	0.030	62	2	6	3.86	0.009

Coordinates (*x*, *y*, *z*) are expressed in millimeters in the Montreal Neurological Institute; *Z* scores result from the statistical parametric analysis; p_{SVC} refers to the probability of the null hypothesis (i.e., absence of activity change associated with spindles), after correction for multiple comparisons on small volumes of interest identified in the literature (references in brackets after the name of each brain area). Additional results that do not survive correction for multiple comparisons can be found in SI Tables 3–5.

Fig. 3*a*). This finding is consistent with the temporal correlation reported in rodents between hippocampal and mesio-frontal neuronal discharges, respectively structured by hippocampal sharp waves/ripples and cortical spindles (24). It would be tempting to relate hippocampal and mesio-frontal activities associated with fast spindles to memory processing. Indeed, power in the fast spindle range (>13 Hz) increases after encoding of hippocampal-dependent declarative memories (25) and after procedural motor learning (26) [but see ref 27 for a memory-related increase in slower spindles (11.25–13.75 Hz)]. However, we did not submit our volunteers to any systematic training session before sleep. We only show that, even without any previous training, both the hippocampus and mesial-frontal cortex are preferentially active during fast, relative to slow, spindles, a condition which could promote their functional interactions.

Table 2. Differential brain responses to slow and fast sleep spindles in stereotactic space

Brain regions	*x*	*y*	*z*	*Z* score	P_{SVC}
	Slow > fast				
Superior frontal gyrus (30)	26	60	32	3.78	0.012
	Fast > slow				
Mesial prefrontal cortex (12)	2	62	−4	3.39	0.042
Orbito-frontal cortex (33)	26	30	−18	3.65	0.019
Middle frontal gyrus (34)	−38	38	28	3.88	0.009
	34	40	26	3.69	0.017
Precentral sulcus (33)	34	−2	50	3.59	0.023
	−32	−6	62	3.43	0.037
Post central gyrus (33)	58	−26	40	3.54	0.027
Anterior insula (33)	32	18	0	3.60	0.022
Hippocampus (34)	−28	−32	−16	3.66	0.019

Statistical results are presented as described in Table 1.

Activity Associated with Slow and Fast Spindles in Thalami and Other Subcortical Structures. The activities associated with fast and slow spindles were much less distinct in thalami than in the cortex. Slow spindles were associated with increased activity in the bulk of both thalami. For fast spindles, the situation was more complex. They elicited significant response only as observed in the common thalamic activation pattern, restricted to lateral and posterior part of both thalami. However, at a lower statistical threshold, an increased activity was detected in a large part of both thalami. This finding explains why no significant difference could be revealed between slow and fast spindles. A cautious interpretation of the results would conclude that the major part of both thalami is recruited during both fast and slow spindles although to variable extent. This interpretation is consistent with cellular recordings that suggest that TC and reticular thalamic neurons constitute two different populations, each characterized by fairly homogeneous cellular properties (23). Consequently, thalamic populations are thought to be able to generate a continuum of frequencies, rather than two separate frequencies. The reason why the activity of lateral and posterior parts of thalami is preferentially associated with fast spindles remains speculative. We assume that the cortical areas which connect to the corresponding thalamic nuclei might contribute to modulate spindle-related activity. We found that the anatomical connectivity of thalamic peak voxels supported this hypothesis. Peak thalamic voxels associated with slow spindles were primarily located in areas compatible with the mediodorsal nucleus (8), and had a high probability of connection with prefrontal cortex (9). In contrast, peak voxels related to fast spindles were additionally compatible with the ventral posterior lateral and pulvinar nuclei (8) and were likely to connect to primary sensorimotor, premotor, and posterior parietal cortices (9) (cf. SI Table 6).

In addition, we observed a significant relationship between the activity in peak thalamic voxels for slow spindles and superior frontal gyrus and between the activity recorded in peak thalamic

NEUROSCIENCE

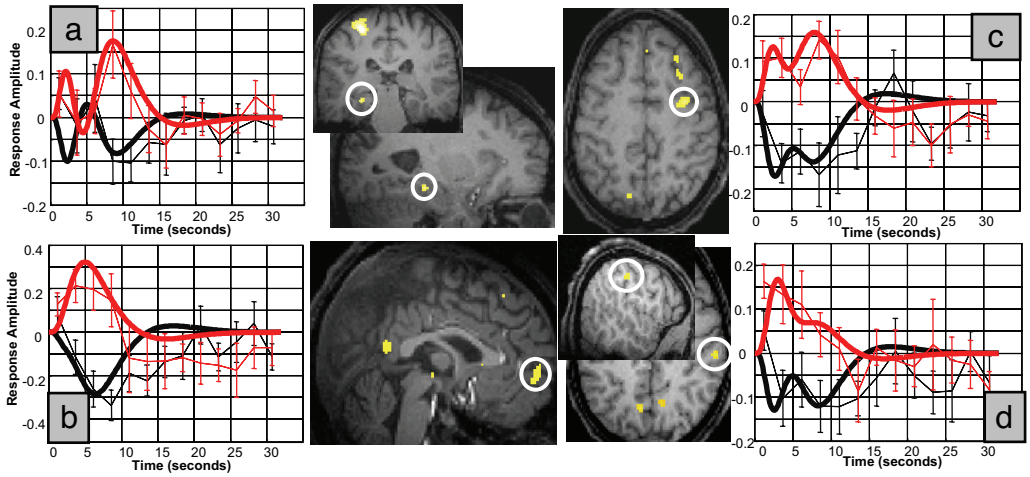

Fig. 3. Differential fMRI activity between fast and slow spindles. Larger brain responses for fast (red) than slow (black) spindles were revealed in the hippocampus (*a*), mesial prefrontal cortex (*b*), precentral gyrus (*c*), and postcentral gyrus (*d*). Peristimulus time histograms show mean response of the corresponding voxels (dotted lines; error bars show SEM) and the corresponding fitted responses (continuous lines).

voxels for fast spindles and cingulate motor zones and SMA. A detailed characterization of the neural firing patterns in these TC loops at the cellular level is required to confirm this hypothesis.

Significant responses associated with slow spindles in basal forebrain/hypothalamus and midbrain tegmentum were unexpected, because it is known that their activity prevents spindle generation through direct cholinergic projections to the thalamus (28). The spatial resolution of fMRI does not allow to assign the detected signal to any given subpopulation of neurons. Nevertheless, our results show that basal forebrain and midbrain tegmentum are systematically recruited during slow spindles. Whether this recruitment is necessary for spindle generation (possibly in relation with spindle termination) or is a mere corollary of TC oscillations should be further characterized at the cellular level. Likewise, the cerebellum has never been specifically implicated in spindle generation although it is in position to modulate thalamic activity through direct cerebello-thalamic projections (29). Further research should therefore specify its functional participation in slow spindles.

Methodological Issues. Our results describe increased regional brain activity in association with spindles and contrast with decreases in regional cerebral blood flow and glucose metabolism reported during light NREM sleep (12, 13, 30) or in relation to sigma power (2) with positron emission tomography. Although the latter technique characterized the hemodynamic and metabolic changes averaged over tens of seconds, fMRI because of its better temporal resolution, was sensitive to transient increases in brain activity associated with spindles and their corresponding neural events, relative to baseline activity of light NREM sleep. However, fMRI data analysis is based on multiple regressions and is sensitive only to consistent increases in activity associated with spindles. In contrast to EEG studies (18), it is blind to the particular temporal dynamics of neural activity during any given spindle.

On the other hand, fMRI benefits of a good spatial resolution and is sensitive to the activity in deep brain structures which can only be inferred by source reconstruction in scalp EEG or MEG data (5, 21). However, assigning activation sites to microscopic neuronal ensembles or nuclei remains uncertain. For instance, the probability of detecting activation in the reticular nucleus was small although the nucleus is deeply involved in spindle generation.

Conclusions

Spindles are the hallmark of light NREM sleep and represent spontaneous events, the neural basis of which are described in detail in animals at the cellular level. Using simultaneous EEG/fMRI, we were able to identify the cerebral correlates of spindles in non-sleep-deprived normal volunteers. As a rule, and in contrast to previous neuroimaging studies, spindles were associated with transient increases in regional brain activity. In addition, we were able to specify both commonalities and differences in brain responses to slow and fast spindles. Intriguingly, we observed substantial differences in cortical, rather than thalamic, activity between the two spindle types. These findings corroborate the existence of two spindle types during human NREM sleep and suggest that fast spindles participate in processing sensorimotor and mnemonic information.

Materials and Methods

Population. Participants were healthy, young subjects ($n = 25$; 11 females; mean age, 21.96). A semistructured interview established the absence of medical, traumatic, or psychiatric history, and of sleep disorders. All participants were nonsmokers, moderate caffeine and alcohol consumers and none were on medication. Participants gave their written informed consent and received a financial compensation for their participation. The study was approved by the Ethics Committee of the Faculty of Medicine of the University of Liège.

Volunteers followed a 4-day constant sleep schedule before their first visit to the laboratory and were not sleep-deprived. Compliance to the schedule was assessed by using a wrist actigraphy (Actiwatch; Cambridge Neuroscience, Cambridge, U.K.) and sleep diaries. Volunteers were requested to refrain from all caffeine and alcohol-containing beverages and intense physical activity for 3 days before participating in the study.

EEG Acquisition and Analysis. EEG was recorded by using two MR-compatible 32-channel amplifiers (Brainamp MR plus; Brain Products, Gilching, Germany) and a MR-compatible EEG cap (Braincap MR; Falk Minow Services, Herrsching-Breitbrunn, Germany) with 64 ring-type electrodes. EEG caps included 62 scalp electrodes that were online referenced to FCz, and one electrooculogram and one electrocardiogram channel. EEG was digitised at 5,000 Hz sampling rate with a 500-nV resolution. Data were analog-filtered by a bandlimiter low pass filter at 250 Hz (30 dB per octave) and a high pass filter with 10-sec time constant corresponding to a high pass frequency of 0.0159 Hz. Data were transferred outside the scanner room through fibre optic cables to a personal computer where the EEG system running Vision Recorder Software v1.03 (Brain Products) was synchronized to the scanner clock. For analysis, EEG data were low-pass filtered (finite impulse

response filter, −36 dB at 70 Hz), down-sampled to 250 Hz, and re-referenced to linked mastoids. Scanner artefacts were removed in Vision Analyzer software, using an adaptive average subtraction (31). Ballistocardiographic artefacts were removed by using an algorithm based on independent component analysis (32). Sleep staging followed standard criteria, and identified periods of stage 2 and stage 3 sleep, free of any artifact, during which the EEG and fMRI data were analyzed. Sleep spindles were automatically detected on Cz (7). For slow spindle detection, data were bandpass filtered between 11 and 13 Hz, using linear phase finite impulse response filters (−3 dB at 11.1 and 12.9 Hz). The root mean square of the filtered signal was calculated by using a time window of 0.25 sec. Sleep spindles were identified by thresholding the spindle root mean square signal at its 95th percentile. The same procedure was followed for detecting fast spindles, using a band pass filter of 13–15 Hz (−3 dB at 13.1 and 14.9 Hz).

fMRI Data Acquisition and Analysis. Functional MRI time series were acquired by using a three-Tesla MR scanner (Allegra; Siemens, Erlangen, Germany). Multislice T2*-weighted fMRI images were obtained with a gradient echo-planar sequence, using axial slice orientation (32 slices; voxel size, $3.4 \times 3.4 \times 3$ mm^3; matrix size, $64 \times 64 \times 32$; repetition time (TR) = 2460 ms; echo time (TE) = 40 ms; flip angle = 90°; field of view = 220 mm; delay = 0). Subjects were scanned during the first half of the night, starting at around midnight. They stayed until they indicated by button press that they would like to go out, or for a maximum of 4,000 scans (≈164 min). The number of scans acquired varied between 1,870 and 4,000 (2,770 ± 852 scans or 113.6 min ± 34.9 min [mean ± SD]). A structural T1-weigthed 3D MP-RAGE sequence (TR = 1,960 ms; TE = 4.43 ms; inversion time, 1,100 ms; field of view, 230×173 mm^2; matrix size, $256 \times 192 \times 176$; voxel size, $0.9 \times 0.9 \times 0.9$ mm) was also acquired in all subjects.

Functional volumes were analyzed by using Statistical Parametric Mapping 5 (SPM5; www.fil.ion.ucl.ac.uk/spm/software/spm5). The series of consecutive fMRI volumes corresponding to a chosen sleep period were selected from the complete fMRI time series and constituted a session (cf. SI Fig. 4). Selected fMRI time series were corrected for head motion, spatially normalized (two-dimensional spline; voxel size, $2 \times 2 \times 2$ mm^3) to an echo planar imaging template conforming to the Montreal Neurological Institute space, and spatially smoothed with a Gaussian Kernel of 8 mm FWHM. The analysis of fMRI data, based on a mixed effects model, was conducted in two serial steps, accounting respectively for intraindividual (fixed) and interindividual (random effects) variance. For each subject, the vectors including the spindle onsets (slow and fast) were convolved with the three canonical basis functions (hemodynamic response function, its derivative and dispersion), and used as regressors in the individual design matrix. The square root of the energy of the signal in the 0.5–4 Hz frequency band was averaged over each repetition time, convolved with the hemodynamic response function and included as another regressor. Movement parameters estimated during realignment (translations in x, y, and z directions and rotations around x, y, and z axes) and a constant vector were also included in the matrix as a variable of no interest. Serial correlations in fMRI signal were estimated by using an autoregressive (order 1) plus white noise model and a restricted maximum likelihood algorithm. The effects of interest were then tested by linear contrasts (main effects of each spindle type, differential response between spindles types), generating statistical parametric maps [(SPM(T)]. The resulting contrasts images were then further smoothed (6 mm FWHM Gaussian Kernel) and entered in a second-level analysis. The second-level analysis consisted of an analysis of variance with the three basis functions and two spindle types as factors. The error covariance was not assumed independent between regressors and a correction for nonsphericity was applied. The resulting set of voxel values constituted maps of F statistics [SPM(F)]. To correct for multiple comparisons, results are reported in *a priori* regions of interest previously identified in neuroimaging studies of NREM sleep (12, 13, 30, 33, 34) on small spherical volumes (10 mm sphere, i.e., ≈4,000 mm^3; SVC). Conjunction analysis used SPMs of the minimum T-statistic over the two spindle main effects, using the conjunction null hypothesis (35), which requires significant regions to be present in all tested conditions (i.e., a logical "AND" conjunction). As above, inferences were based on P values adjusted for the search volume using random field theory. Probabilities of thalamus connectivity were derived from the online available thalamus connectivity atlas, which is based on diffusion tensor imaging (www.fmrib.ox.ac.uk/connect) (9).

A more detailed description of materials and methods and thalamic connectivity data can be found in the *SI Materials and Methods*.

This study was supported by the Belgian Fonds National de la Recherche Scientifique (G.V., E.B., M.B., T.D., M.D., C.P., G.R., A.D., V.S. and P.M.), the Fondation Médicale Reine Elisabeth, the Research Fund of ULg, PAI/IAP Interuniversity Pole of Attraction P5/04, a PhD grant from the French Ministère de la Recherche (to G.A.), an Emmy Noether Fellowship from the German Research Foundation (to S.G.), and an Austrian Science Fund Erwin-Schrödinger Fellowship J2470-B02 (to M.S.).

1. Steriade M, McCarley RW (2005) *Brain Control of Wakefulness and Sleep* (Kluwer Academic, New York).
2. Hofle N, Paus T, Reutens D, Fiset P, Gotman J, Evans AC, Jones BE (1997) *J Neurosci* 17:4800–4808.
3. De Gennaro L, Ferrara M (2003) *Sleep Med Rev* 7:423–440.
4. Bodizs R, Kis T, Lazar AS, Havran L, Rigo P, Clemens Z, Halasz P (2005) *J Sleep Res* 14:285–292.
5. Anderer P, Klösch G, Gruber G, Trenker E, Pascual-Marqui RD, Zeitlhofer J, Barbanoj MJ, Rappelsberger P, Saletu B (2001) *Neuroscience* 103:581–592.
6. Zygierewicz J, Blinowska KJ, Durka PJ, Szelenberger W, Niemcewicz S, Androsiuk W (1999) *Clin Neurophysiol* 110:2136–2147.
7. Mölle M, Marshall L, Gais S, Born J (2002) *J Neurosci* 22:10941–10947.
8. Morel A, Magnin M, Jeanmonod D (1997) *J Comp Neurol* 387:588–630.
9. Behrens TE, Johansen-Berg H, Woolrich MW, Smith SM, Wheeler-Kingshott CA, Boulby PA, Barker GJ, Sillery EL, Sheehan K, Ciccarelli O, *et al.* (2003) *Nat Neurosci* 6:750–757.
10. Steriade M, Parent A, Hada J (1984) *J Comp Neurol* 229:531–547.
11. Pare D, Steriade M, Deschenes M, Oakson G (1987) *J Neurophysiol* 57:1669–1685.
12. Maquet P, Degueldre C, Delfiore G, Aerts J, Peters JM, Luxen A, Franck G (1997) *J Neurosci* 17:2807–2812.
13. Braun AR, Balkin TJ, Wesenten NJ, Carson RE, Varga M, Baldwin P, Selbie S, Belenky G, Herscovitch P (1997) *Brain* 120(Pt 7):1173–1197.
14. Giguere M, Goldman-Rakic PS (1988) *J Comp Neurol* 277:195–213.
15. Portas CM, Krakow K, Allen P, Josephs O, Armony JL, Frith CD (2000) *Neuron* 28:991–999.
16. Cote KA, Epps TM, Campbell KB (2000) *J Sleep Res* 9:19–26.
17. Nakamura M, Uchida S, Maehara T, Kawai K, Hirai N, Nakabayashi T, Arakaki H, Okubo Y, Nishikawa T, Shimizu H (2003) *Neurosci Res* 45:419–427.
18. Doran S (2003) *Sleep Res Online* 5:133–139.
19. Hari R, Salmelin R (1997) *Trends Neurosci* 20:44–49.
20. Pineda JA (2005) *Brain Res Rev* 50:57–68.
21. Manshanden I, De Munck JC, Simon NR, Lopes da Silva FH (2002) *Clin Neurophysiol* 113:1937–1947.
22. Sterman MB, Howe RC, Macdonald LR (1970) *Science* 167:1146–1148.
23. Steriade M, Amzica F (1998) *Sleep Res Online* 1:1–10.
24. Siapas AG, Wilson MA (1998) *Neuron* 21:1123–1128.
25. Schabus M, Hödlmoser K, Gruber G, Sauter C, Anderer P, Klösch G, Parapatics S, Saletu B, Klimesch W, Zeitlhofer J (2006) *Eur J Neurosci* 23:1738–1746.
26. Milner CE, Fogel SM, Cote KA (2006) *Biol Psychol* 73:141–156.
27. Schmidt C, Peigneux P, Muto V, Schenkel M, Knoblauch V, Munch M, de Quervain DJ, Wirz-Justice A, Cajochen C (2006) *J Neurosci* 26:8976–8982.
28. McCormick DA, Bal T (1997) *Annu Rev Neurosci* 20:185–215.
29. Calzavara R, Zappala A, Rozzi S, Matelli M, Luppino G (2005) *Eur J Neurosci* 21:1869–1894.
30. Kajimura N, Uchiyama M, Takayama Y, Uchida S, Uema T, Kato M, Sekimoto M, Watanabe T, Nakajima T, Horikoshi S, *et al.* (1999) *J Neurosci* 19:10065–10073.
31. Allen PJ, Josephs O, Turner R (2000) *NeuroImage* 12:230–239.
32. Srivastava G, Crottaz-Herbette S, Lau KM, Glover GH, Menon V (2005) *NeuroImage* 24:50–60.
33. Kaufmann C, Wehrle R, Wetter TC, Holsboer F, Auer DP, Pollmacher T, Czisch M (2006) *Brain* 129:655–667.
34. Nofzinger EA, Buysse DJ, Miewald JM, Meltzer CC, Price JC, Sembrat RC, Ombao H, Reynolds CF, Monk TH, Hall M, *et al.* (2002) *Brain* 125:1105–1115.
35. Nichols T, Brett M, Andersson J, Wager T, Poline JB (2005) *NeuroImage* 25:653–660.